

Stable Throughput Tradeoffs in Cognitive Radio Networks

S. Kompella,¹ G.D. Nguyen,¹ J.E. Wieselthier,² and A. Ephremides³

¹Information Technology Division

²Wieselthier Research

³University of Maryland

Introduction: This work introduces a highly innovative approach for the operation of cognitive radio networks that is suitable for tactical wireless environments and provides a rigorous analysis of tradeoffs in network throughput that enables improved system performance. Cognitive wireless network technology, which integrates adaptive algorithms, dynamic spectrum access, and channel sensing, has the potential to provide significant gains in communication capability to warfighters. To achieve the needed performance improvements and avoid disruptions, cognitive radios offer tremendous opportunities for adaptation. Systems will have the capability to sense the conditions of their local operating environment and then dynamically adapt their data rate, modulation, coding, transmit power, and frequency, as needed, to changes in propagation, signal fading, multipath, or friendly/unfriendly interference.

Although there has been considerable research and development in the area of cognitive radios in recent years, few studies have addressed the challenges of forming cognitive radio networks. Consequently, issues associated with cognitive tactical wireless networks have scarcely been addressed. The present work addresses fundamental issues in cognitive shared channels where the users have different priority levels, a situation that is commonly seen in tactical edge networks. This work is being carried out as part of the Office of the Secretary of Defense (OSD) Networked Communications Capabilities Program (NCCP), and is in line with the Navy/Marine Corps evolving strategic plan and priorities.

System Model and Analysis: In the prevailing paradigm of operation for cognitive radios, “secondary” (lower priority) users are required to sense idle periods during which the “primary” (higher priority) users are not transmitting, and transmit their own data during such idle periods, so as to not cause interference to primary users. Furthermore, the secondary users are required to cease transmission when a primary user is detected in a channel.

The present work departs from this standard model by permitting secondary users to use transmission policies that exploit the multireception capabilities of modern receivers, thereby allowing secondary users to transmit concurrently with primary users (with a transmission probability p), a crucial capability for future

tactical networks. In the simplest (noncooperative) mode of operation, the secondary users’ performance is optimized by choosing the appropriate value of p . An enhanced cooperative mode of operation is then developed in which secondary users can serve as relays for unsuccessful packets transmitted by primary users (see Fig. 1). In this cooperative mode, a tradeoff arises when the secondary node is activated along with the primary so that both transmissions may be successful, but with a lower probability, compared with the case of the secondary node staying idle when the primary user transmits.

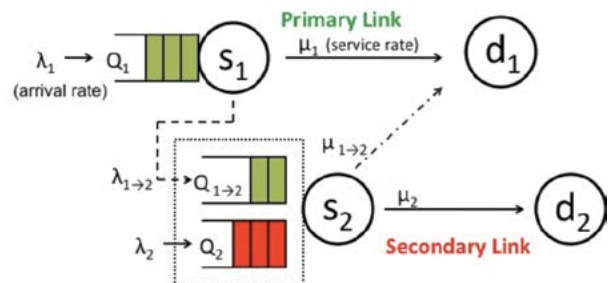


FIGURE 1

Cognitive radio network model. s_1 = primary user; s_2 = secondary user; d_1 = primary destination; d_2 = secondary destination; λ = arrival rate; Q = queue length; μ = service rate.

The computation of the stable throughput region of a network with one primary user and one secondary user (i.e., the set of input data rates that can be supported by the primary and secondary user, while maintaining finite queues) is an intractable problem because it is characterized by interacting packet queues. This work, therefore, uses the queueing-theoretic notion of “stochastic dominance” to construct a “dominant system” in which the queues do not interact with each other, and whose stability region inner-bounds that of the original system. It is shown that the dominant system and the original system behave identically at the boundary of the stability region. Therefore, the dominant system, whose analysis is tractable, is used to determine the stability region of the original (intractable) system.

Results: The ensuing analysis^{1,2} shows that the appropriate behavior of secondary users (secondary cooperation) not only provides improved service for the secondary users, but actually provides better performance for the primary user than that which would be achieved even if no secondary users were competing for channel access, as can be observed in Fig. 2. This key insight has far-reaching implications in tactical and commercial environments alike. Furthermore, analyzing the impact of the knowledge of secondary users’ channel state information³ (queue states, channel conditions, etc.) on the stable throughput region illustrates

that such knowledge benefits the entire network in terms of improved throughput region, much more than cooperation alone.

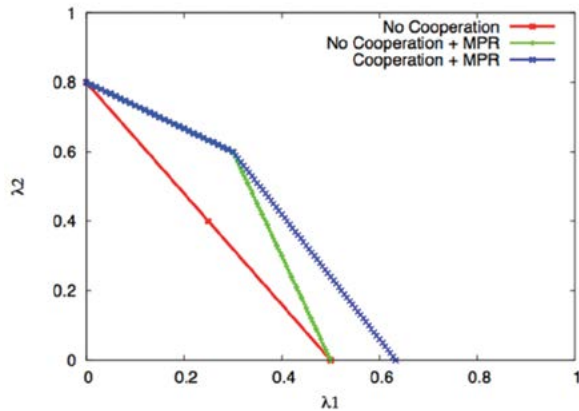


FIGURE 2 Comparison of the stability regions of the noncooperation and the cooperation schemes (MPR = multipacket reception).

Summary: The main contributions of this work are the development of a cooperative cognitive radio networking technique that provides improved performance for both the primary and secondary user, and the development of a rigorous mathematical model that enables the evaluation of performance tradeoffs that will lead to the improved performance of realistic tactical communication networks.

[Sponsored by the NRL Base Program (CNR funded)]

References

- ¹ S. Kompella, G.D. Nguyen, J.E. Wieselthier, and A. Ephremides, "Stable Throughput Tradeoffs in Cognitive Shared Channels with Cooperative Relaying," in *2011 Proceedings IEEE INFOCOM* (IEEE, Piscataway, NJ, 2011), pp. 1961–1969.
- ² S. Kompella, G.D. Nguyen, C. Kam, J.E. Wieselthier, and A. Ephremides, "Cooperation in Cognitive Underlay Networks: Stable Throughput Tradeoffs," under review, *IEEE/ACM Transactions on Networking*.
- ³ S. Kompella, G.D. Nguyen, J.E. Wieselthier, and A. Ephremides, "Impact of Channel State Information on the Stability of Cognitive Shared Channels," in *2012 Proceedings IEEE INFOCOM* (IEEE, Piscataway, NJ, 2012), pp. 3021–3025.

X-Band Airborne Satellite Communications

T.R. Husson and M.A. Rupal
Information Technology Division

Introduction: The Department of Defense is increasingly reliant upon airborne sensors to provide battlespace information. This means there is a greater

need for sending large amounts of data from these airborne platforms in real time to analysts on the ground. Since the ground stations are often beyond line-of-sight to the aircraft, the use of satellite communications provides the best solution.

L-band (1.5 to 1.6 GHz) commercial satellite communications systems for aircraft have been in use for a long time. However, the data bandwidth provided by these systems is not nearly enough to accommodate the current broadband sensors. The latest airborne L-band system from Inmarsat (SwiftBroadband) provides a maximum data rate of 432 kbps, which is insufficient for streaming video and other high-bandwidth sensors. X-band (8 GHz) provides the required bandwidth for these applications, and spectrum is available on military satellites and from a limited number of satellite providers.

This article describes the testing of an airborne X-band satellite communications system. Bandwidths of 10 MHz from the air to a small (2.4 m) ground station antenna were demonstrated. Figure 3 shows the communications architecture. The testing was conducted in the vicinity of Hagerstown, Maryland.

Communications System: The airborne system consisted of a tracking antenna, satellite modem, voice-over-IP (VoIP) adapter, laptop computer, and a spectrum analyzer (for RF measurements). The test aircraft was a Beechcraft King Air A2000. The EMS AS-X Wavestorm airborne antenna system provided 27 to 28 dB of gain (equivalent to a 0.4 m dish antenna). The antenna system was able to track the satellite throughout the aircraft maneuvers using an integrated attitude and heading reference system (AHRS) and global positioning system (GPS) receiver.

Two different satellite modems were tested. Both the Paradise Quantum 20 and the Newtec EL470 used standard DVB-S2 waveforms and error coding and had the capability to log lock status, signal level, and Eb/No (signal quality).

The ground station was set up at the Intelsat Mountainside Teleport in Hagerstown. The antenna was a GATR 2.4 m portable X-band antenna. The antenna included an integrated block downconverter and low-noise amplifier for the receive signal, and an integrated block upconverter and power amplifier for the transmit signal. Other equipment at the ground station mirrored the equipment on the aircraft with two different satellite modems, a laptop computer, and a spectrum analyzer.

Test Setup: Two different geostationary satellites were used during the testing to provide different pointing angles. Identical bandwidth channels were used on both satellites. The XTAR-LANT satellite is located at 30° W which required pointing angles of 120.1°

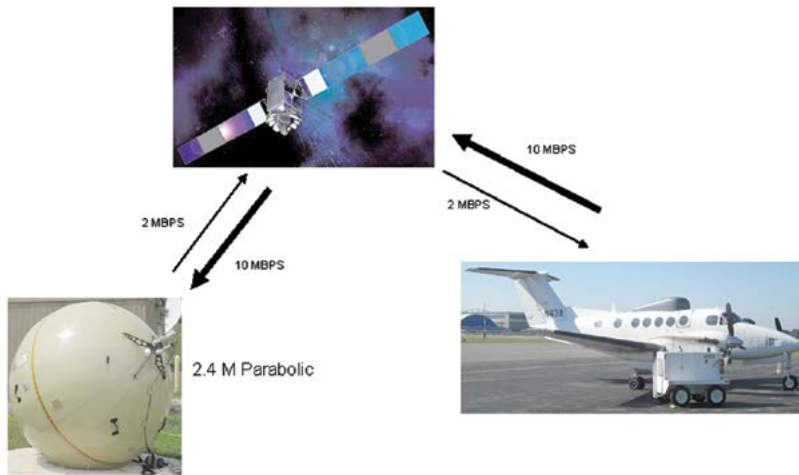


FIGURE 3
Communications architecture for X-band airborne satellite communications testing.

azimuth and 23.3° elevation from Hagerstown. The SKYNET 5C satellite is located at 18° W and required pointing angles of 110.2° azimuth and 14.4° elevation.

A number of applications were used for testing the satellite links (both air-to-ground and ground-to-air). The NRL Multi-Generator (MGEN)¹ was used to test the capacity of the communications links. The software was used both during straight and level flight and during aircraft maneuvers. Transfer of large data files was tested using the open-source FileZilla² server and client software. Streaming of video was tested using the VLC Media Player.³ Real-time data chat was tested using the VSee⁴ collaboration tool, and, remote desktop control was implemented using the TightVNC⁵ software package.

Test Results: Identical channels on both satellites were used with a 10 MHz link from the aircraft and a 2 MHz link to the aircraft. Figure 4 shows the 10 MHz air-to-ground carrier and the 2 MHz ground-to-air carrier as recorded at the ground station. Both satellites provided equivalent performance through the various tests.

Modem logs were recorded both on the ground and in the aircraft during all test flights. The primary parameter of interest from the logs was Eb/No (energy per bit to noise power spectral density ratio). This figure of merit indicates the quality of the signal and is related to the received bit error rate. Figure 5 shows a typical Eb/No plot from the modem on the aircraft.

Both satellite modems were configured for QPSK modulation with half rate forward error correction (FEC) coding. This configuration provides 10 Mbps data transfer across the 10 MHz air-to-ground link. The ability to sustain these data rates was tested and verified using the NRL MGEN software. Figure 6 is a plot from MGEN that shows a sustained 9 Mbps transfer rate from the aircraft. Simultaneously with this sustained transfer rate, a data chat and a VoIP voice call were also in progress. The dropouts on the plot are due to antenna blockage on the aircraft during maneuvers. However, the plot shows the data transfer rate fully restored as soon as the aircraft antenna was able to reacquire lock on the satellite.

The Newtec EL470 satellite modem had an adaptive coding and modulation (ACM) option. The ACM allowed the modem to adapt its data transfer rate and FEC

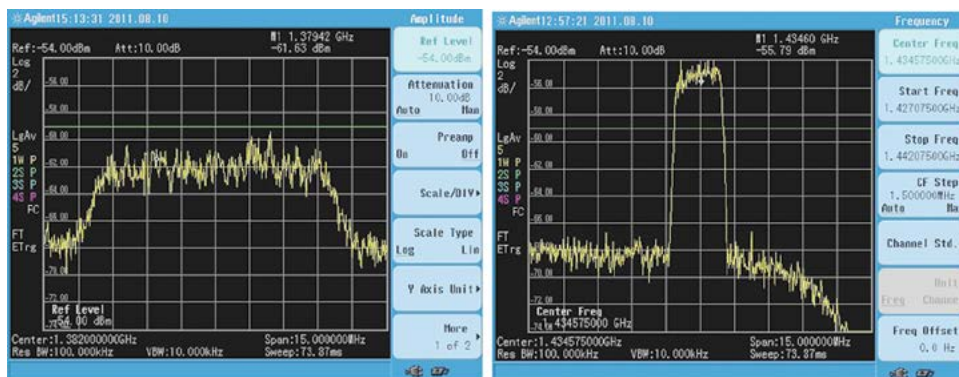


FIGURE 4
Forward and return carrier signals from the satellite.

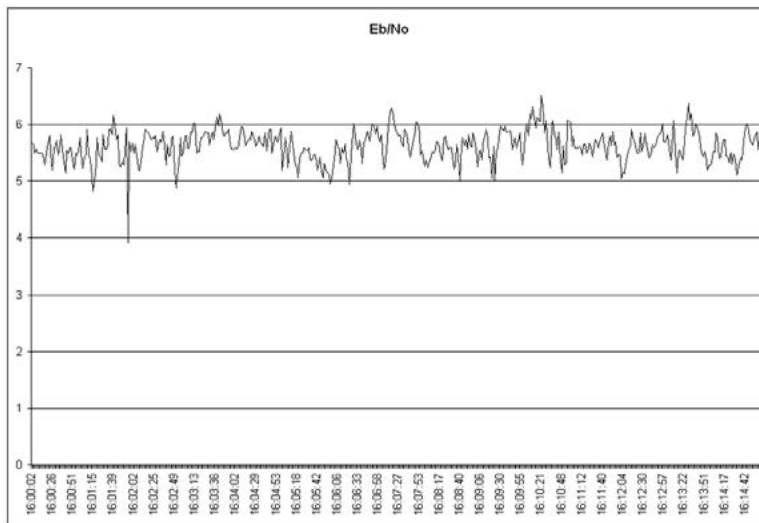


FIGURE 5
Typical Eb/No plot from the aircraft modem.

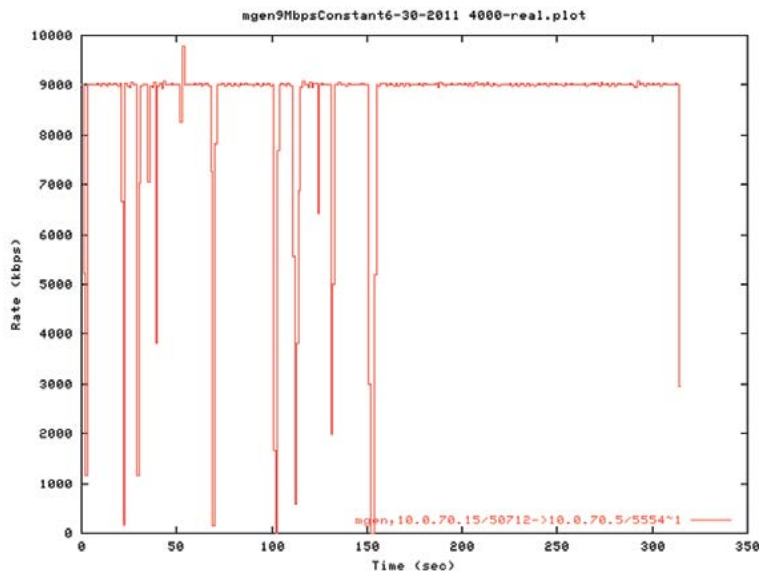


FIGURE 6
MGEN plot of sustained air-to-ground data transfer rate.

coding based on the received signal quality (Eb/No) to make optimal use of the channel. Using the Newtec modem with ACM the aircraft was able to transfer data at rates up to 16 Mbps as measured by the MGEN software.

In addition to the throughput testing using the MGEN software, other data transfer applications were tested. Large file transfers using file transfer protocol (FTP) were initiated in both directions and results showed transfer rates that matched those recorded by the MGEN tests. Multicast streaming video was sent from the aircraft to the ground station during flight. There were brief interruptions of the stream due to antenna blockage during aircraft maneuvers, but the

stream was quickly restored when the antenna reacquired lock on the satellite.

VoIP voice calls and real-time data chat applications were used simultaneously during all the higher data rate tests, allowing close coordination between the operators on the aircraft and at the ground station.

Also demonstrated during the tests was the ability of the ground station operator to remotely control the laptop computer on the aircraft using the TightVNC software.

Summary: During a series of flight tests, the ability to maintain a consistent 10 Mbps/2 Mbps link between the airborne terminal and a ground station using a 2.4

m antenna was demonstrated. The airborne antenna demonstrated the ability to track two different satellites including one at a low elevation angle (14.4°). Two different satellite modems were successfully tested at these data rates. Using the ACM on the Newtec modem, a higher data rate was achieved.

The availability of X-band spectrum on several different satellites provides the DoD with the flexibility to deploy various airborne sensors and send high-bandwidth data in real time to ground-based analysts.

[Sponsored by Cold Regions Research and Engineering Laboratory, U.S. Army Corps of Engineers]

References

¹ <http://cs.itd.nrl.navy.mil/work/mgen/>

² <http://filezilla-project.org/>

³ <http://www.videolan.org/vlc/>

⁴ <http://vsee.com/>

⁵ <http://www.tightvnc.com/>

GLADIS Hosted Payload Demonstrates Nanosatellite Technology

J. Middour,¹ I. Galysh,¹ K. Clark,¹ T. Rodillos,¹ M. Haffner,¹ C. Belmonte,¹ R. Baummer,¹ J. Graham,² and J. Tugman³

¹*Space Systems Development Department*

²*Three Lions Consulting, LLC*

³*JTM & Associates, Inc.*

Overview: NRL's Space Systems Development Department completed development and testing of a hosted payload system intended to demonstrate key technologies for very small satellites. So-called "nano" satellites, typically less than 10 kg, are of interest for their potential to fulfill certain scientific and military missions at greatly reduced cost for manufacture and launch to orbit. The Global Awareness Data-Extraction International Satellite hosted payload, GLADIS for short, was conceived, designed, and built by the Space Systems Development Department (Fig. 7). It is due to be launched to the International Space Station in 2013 for a one-year, in-orbit evaluation of a two-way UHF communications capability using specially developed structures, electronics, and antennas.

History: The GLADIS hosted payload stemmed from a concept for a space-based infrastructure comprised of many small satellites providing a communications backbone to control and manage autonomous, distributed, unattended sensors and unmanned vehicles which are increasingly employed to monitor the unwired regions of the Earth for improved scien-

tific, environmental, safety, and security awareness.¹ As envisioned, a GLADIS constellation would employ a network of simple ground terminals, up to 30 nanosatellites, and an efficient command and control service to extract the maximum communications capacity from many small and low-power satellites. As built, the GLADIS hosted payload will prove key technological elements required for the full constellation, including small satellite structural and power systems, low-power electronics, and very small antenna arrays suited for space communications. The demonstration will also test an enterprise command and control system along with very small, low-power, satellite-to-ground communications terminals.



FIGURE 7
The NRL GLADIS team with the flight payload.

Key Development Attributes: The GLADIS Data Extraction payload evolved from the Ocean Data Telemetry Microsatellite Link (ODTML) experiments flown and tested sequentially on TacSat-3, STPSat-2, and TacSat-4. The Data-X transmitter/receiver operates around 401 MHz to provide two-way data relay from ocean and terrestrial sensors to users via Internet connection. The UHF frequency is suitable for low power and is also good for foliage penetration. The Data-X payload transmits queries to small, low-power communication terminals attached to unattended sensors and receives sensor-collected data in reply at digital bit rates of 2400 to 9600 bits per second. The payload enables data exfiltration and infiltration to remote sensors of any kind, such as ocean sensors, unattended ground sensors, or portable radios. Two-way communication allows acknowledgments and error correction. The data handling architecture can accommodate thousands of sensors such that tasking can be performed autonomously and data disseminated using the Internet. The UHF ground terminals are low cost, have a simple antenna that does not require pointing, and their sleep

mode saves power. Both ground and space segments are customizable via reprogrammable software, including while on orbit.

The GLADIS transceiver uses an antenna, Data-X receiver, Data-X transmitter, field programmable gate array (FPGA), and a general purpose processor (GPP) to perform its data relay mission. The antenna is circularly polarized with four quarter wavelength monopoles phased 90° apart and tilted away from each other. A plastic ring around the bottom of the payload electrically insulates the antenna ground plane, achieving an enhanced beam pattern for ground coverage.² The Data-X receiver filters, amplifies, digitizes the received signal, and feeds it to the FPGA for digital signal processing to demodulate the uplink. The demodulated bit stream goes to the GPP for message decoding and high-level protocol implementation. The GPP also provides sensor handshake and interrogation bit streams back to the FPGA. The FPGA implements a binary-phase-shift-keyed control signal to the Data-X transmitter for modulation. The transmitter uses a digital-to-analog converter for modulation, along with a frequency mixer and amplifiers to transmit the UHF handshake and interrogation signals to the ground terminals on the sensors.

The GLADIS communications architecture is made up of the enterprise server, the Satellite Operations Center, the operating system, and ground-space comms terminals. “End-to-end” system tests are planned for FY2014.



FIGURE 8
The GLADIS payload attached to STP-H4 in launch configuration.

Summary: The GLADIS hosted payload received funding from the Office of Naval Research, the Department of Homeland Security, and the Department of Defense Space Test Program (STP). It will be shipped to Japan to be loaded aboard a Japanese Space Agency rocket for launch to the International Space Station in

2013. The mission, known as STP-Houston 4 (STP-H4; see Fig. 8), includes GLADIS and two other NRL science payloads: the Small Wind and Temperature Spectrometer (SWATS) and the Miniature Array of Radiation Sensors (MARS), both designed and built by the NRL Space Science Division.

NRL scientists and engineers will use the results of the GLADIS hosted payload demonstration of key technologies for very small satellites to improve the capacity of future satellites while controlling cost and increasing access to space.

[Sponsored by ONR]

References

- ¹J. Middour, J. Mittleman, J. Tugman, J. Graham, S. Thonnard, and F. Hellrich, “Concept for an International Small Satellite Constellation to Monitor Unattended Ground Sensors,” presented at CANEUS 2009, NASA Ames Research Center, Moffett Field, CA, March 2009.
- ²W. Lippincott, “Development of a Deployable UHF Crossed Dipole Antenna Suitable for Nano Satellites,” presented at the ACES Applied Computational Electromagnetics Society 27th International Review of Progress in Applied Computational Electromagnetics, Williamsburg, VA, March 2011.

Dynamic Network Analysis for Mobile (DyNAMo) Adaptation

J. Macker, J. Dean, and D. Claypool
Information Technology Division

Overview: In the Dynamic Network Analysis for Mobile (DyNAMo) adaptation project, NRL’s Protocol Engineering and Advanced Networking Section is conducting research to address novel network design and analysis challenges involving significant mobility, autonomy, and disruptive dynamics. Figure 9 is an overview of the approach and goals of this research.

Commensurate with NRL’s leadership in developing a next generation of mobile network modeling capabilities is our goal of developing new approaches for analyzing dynamic networks to enable further improvements in protocol design, analysis, and adaptation for mobile, autonomous communication networks.

Measurement Tools and Methods: By leveraging high-fidelity mobile network modeling components we have developed, it is possible to examine dynamic communication networks with novel and repeatable methods that reflect real-world deployment conditions. These high-fidelity models and mobile network scenario tools produce dynamic metadata that is stored and manipulated using a network graph language (e.g., graphML). In this way, researchers can capture the state

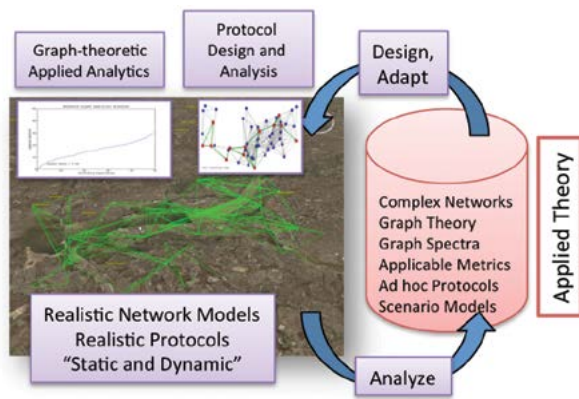


FIGURE 9
Overview of DyNAMo process and goals.

conditions of dynamic autonomous networks under study and perform scenario-driven design and analysis in a repeatable fashion. Dynamic topological metadata examples include metrics related to distributed protocol organization (e.g., algorithm decision state) and environmental state variables (e.g., stochastic node and edge conditions). Recently, this dynamic modeling capability has been applied to studying two specific autonomous networking problems: (1) self-organizing structural stability and (2) temporal detection and tracking of dynamic network structures.

Improving the Stability of Self-Organizing Networks: By applying DyNAMo models, we have achieved temporal stability improvements to distributed connected dominating set (CDS) algorithms. These algorithms are typically used for structural control and efficient data distribution within autonomous mobile networks, such as mobile ad hoc networking technical standards. Such distributed algorithms compute topologically connected control structures within dynamic network topologies, but at present, standard algorithms experience high degrees of membership reelection changes. While such algorithms are needed and beneficial, the topological churn caused by continual reelection has been shown to be significantly problematic in disruptive deployment scenarios such as hybrid airborne-surface communication networks and urban environments. Using DyNAMo techniques and related modeling workflows, we developed both an analytical approach and a recent solution for a well-known distributed algorithm that provides up to 30% to 40% stability improvements under dynamic wireless network conditions. Figure 10 provides an example of such an improvement within a 600-second modeled mobile scenario; stability gains are achieved without additional redundancy in the topological structure, thus improving the performance of related network protocols without sacrificing additional precious wireless bandwidth. We are presently examining the

measurable performance improvements to distributed operations and upper layer applications once increased stability is realized through methods we have developed as discussed in Ref. 1.

Analyzing Evolving Structures in Dynamic Networks: Many networks of interest, including communication and information networks, often naturally evolve or divide into communities or nodal structures over time. This division or evolution can be intentional or may be caused by many factors across layers of a networking architecture, including clustered or constrained motion, physics and environmental effects, and organizational or informational relationships that evolve over time. By identifying the relative strengths and weaknesses of existing network structures, pinpointing critical network locations, and classifying the evolution of clustered relationships, we can better address future dynamic network planning and adaptation challenges, including defense of networks and robust adaptation in disruptive environments.

We have taken a multidisciplinary approach of applying machine learning methods and recent advances in spectral graph theory to both detecting and tracking clusters within autonomous networks over time. Figure 11 depicts the results from autopartitioning and tracking network clusters using graph spectral eigen-decomposition through a 10-minute, 90-node network deployed in a maritime-modeled scenario. The lower graph in Fig. 11 also provides an example of research improvements to dynamic autopartitioning and shows that we can in practice do better than known eigen-based spectral gap techniques.²

The following summarizes recent accomplishments of this work.

- (1) We have applied spectral analysis to mobile network traces to detect, stabilize, and track structural community decomposition.
- (2) We have determined the size of partitions over time using eigendecomposition data along with a usable partition quality metric for dynamic analysis and adaptation purposes.

Future Work: This work demonstrates the use of high-fidelity mobile network modeling and associated analytics to detect and research dynamic network conditions and protocols to improve an understanding of performance in the research, planning, and deployment stages. Future work will address additional challenges of real-time analysis and adaptation of complex, autonomous networks based upon associated applied analytics.

[Sponsored by the NRL Base Program (CNR funded)]

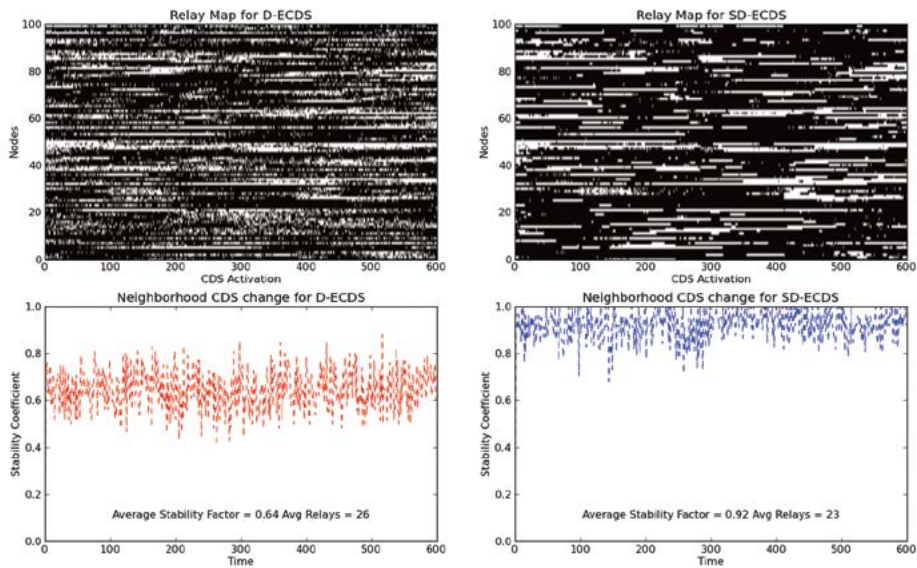


FIGURE 10
Graph of CDS stability improvement results using DyNAMo evolving graph models.

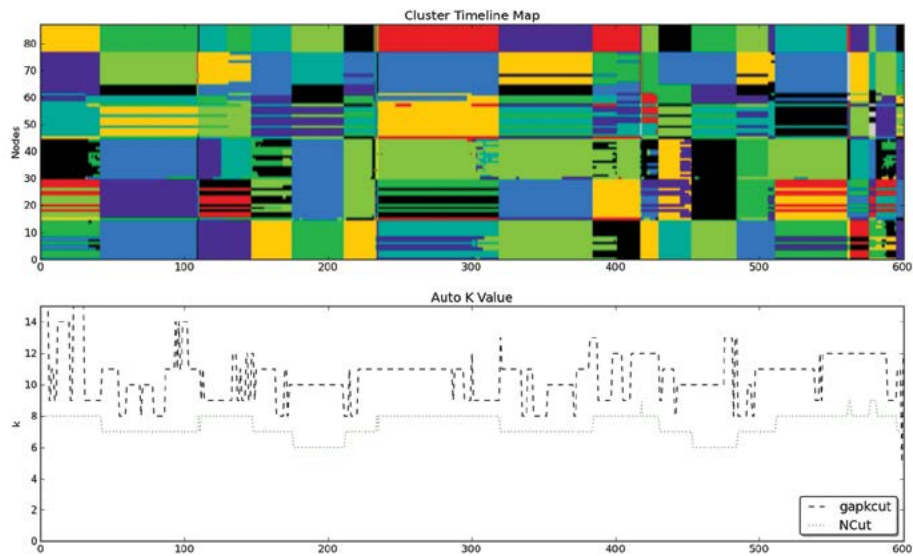


FIGURE 11
Color map illustrating dynamic cluster detection and tracking.

References

- ¹J.P. Macker, B. Adamson, and D.J. Claypool, “Temporal Stability for Dynamic Network Relay Sets,” in Proceedings MILCOM 2012, Orlando, FL, Oct. 29–Nov. 1, 2012; doi:10.1109/MILCOM.2012.6415615.
- ²J.P. Macker and D.J. Claypool, “Dynamic Communities in Evolving Network Graphs,” in Proceedings MILCOM 2012, Orlando, FL, Oct. 29–Nov. 1, 2012; doi:10.1109/MILCOM.2012.6415614.

Frequency Position Modulation

J. Goodman, C. Bertocini, B. Nousain, and G. Cowart
Tactical Electronic Warfare Division

Introduction: NRL has developed a novel, high data, low probability of intercept (LPI) and low probability of detection (LPD) waveform called Frequency Position Modulation (FPM). Each symbol in an FPM waveform is represented by multiple tones that are

spread over an extremely wide instantaneous bandwidth (IBW). Wideband operation enables FPM to achieve higher data rates than conventional LPI/LPD communications without as significant a sacrifice in processing gain. FPM processing is novel in two key respects. The first is that multiple local oscillators (LOs) are simultaneously used at the receiver in the downconversion process to collapse a wideband spectrum into a much narrower one. This enables a single receiver to digitize a wider bandwidth at its input than is normally possible using standard Nyquist sampling. Second, nonlinearities generated by the power amplifier (PA) in the transmitter — which are typically unwanted artifacts — are exploited by FPM demodulation on receive to reduce the symbol error rate (SER). We compare the SER vs signal-to-noise ratio (SNR) of FPM against a common LPI/LPD waveform, direct sequence-code division multiple access (DS-CDMA), and demonstrate nearly an order of magnitude improvement in performance.

FPM Constellation and Symbol Transmission:

Each symbol in an FPM waveform¹ is composed of a discrete set of N_{pos} tones. Each of the N_{pos} tones is spread far apart in frequency to mitigate fading and interference. The tones are positioned in frequency such that when they are mixed with multiple LOs on receive, the symbols collapse into a narrower bandwidth, enabling the use of an undersampling analog-to-digital converter (ADC).

A simple procedure for choosing the frequency locations of the symbols is illustrated in Fig. 12, where each colored group corresponds to a contiguous set of baseband frequencies. From each group, a single tone is selected to generate an FPM symbol. In Fig 12, with $N_{pos} = 4$, the LO and frequency support of the colored groups are selected so that the symbols collapse into a narrower band than the one in which they were transmitted.

To calculate the exact frequencies, we need to define the number of samples per symbol, N_{smp} . The choice of N_{smp} is a trade of data rate against processing gain, e.g., the more samples per symbol, the higher the processing, but the lower the data rate. In each colored group there are M frequencies and the number of symbols that share a common frequency component is represented by q ; we represent the FPM constellation as $M_{q,N_{pos}}$. The selection of q is a tradeoff between SER and data rate; two different values are compared in the results section.

At baseband the tones are shaped to promote or suppress nonlinearities generated by the PA.² The nonlinearities that are promoted appear as additional tones, so they increase the Hamming distance and therefore decrease SER for a fixed SNR. A block diagram of the

transmitter is illustrated on the left-hand side of Fig. 13. FPM symbol integrity is not adversely affected by driving the PA into saturation to generate nonlinearities enabling power efficient operation.

FPM Demodulation: The received signal is passed through a fixed comb filter after the low-noise amplifier (LNA) to isolate the $N_{pos} \times M$ frequency locations in the spectrum where the symbols have support, as illustrated on the right-hand side of Fig. 13. The symbols may in fact be spread out over many GHz of instantaneous bandwidth. Therefore, to recover the symbols using a single receiver, $N_{pos}/2$ LOs are added together to mix the incoming signal down to baseband. This process is illustrated in Fig. 14 for the case in which $N_{smp} = 2048$, $N_{pos} = 4$, and $M = 64$, effectively collapsing the spectrum into one-quarter the original bandwidth. Unlike compressed sensing,³ collapsing the wideband spectrum into a narrower one does not suffer from noise folding and loss of SNR.

Demodulation takes place in the frequency domain using a fast Fourier transform (FFT) matched filter. Maximum likelihood (ML) or maximum *a posteriori* (MAP) demodulation techniques are then used to recover symbols embedded in noise and subject to Rayleigh fading. To supplement these techniques, we also developed a statistical demodulator based on a Hamming distance metric for the case when FPM operates in a spectrally crowded environment and is subject to unexpected interference. In this case, with sufficient SNR, the nonlinearities offer a distinct advantage by increasing the Hamming distance. For example, the minimum Hamming distance of a $64_{2,4}$ -ary constellation increased from 3 to 8 when nonlinearities were exploited, albeit the inherently lower SNR of the distortions prevented their complete exploitation. The performance of each of these techniques is presented in the next section.

Results: The efficacy of FPM was tested by running Monte Carlo simulations of a communications system using $64_{1,4}$ - and $64_{2,4}$ -ary FPM and comparing its SER performance against that of DS-CDMA with BPSK modulation and ML demodulation. The results of this comparison are plotted in Fig. 15. Each of the waveforms was subject to additive white Gaussian noise and Rayleigh fading, as well as random narrowband interference. DS-CDMA and $64_{2,4}$ -ary FPM were parameterized to maintain identical data rates to one another for the performance comparison, while $64_{1,4}$ -ary operated at half the data rate.

When FPM was not subject to interference (SIR = ∞ , $E(N_s) = N_s = 0$), FPM ML demodulation outperformed DS-CDMA. When interference was present, FPM with statistical demodulation using a Hamming

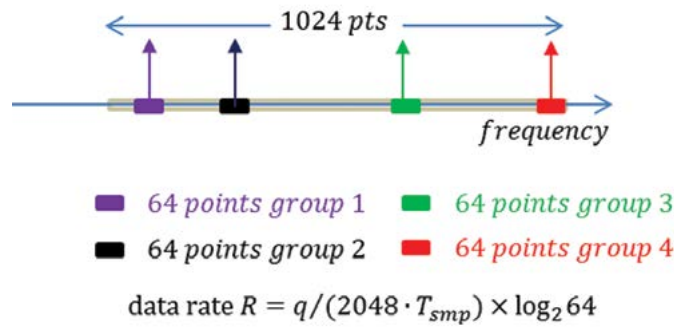


FIGURE 12
 An example FPM $64_{q,4}$ -ary constellation, where $N_{smp} = 2048$, $N_{pos} = 4$, $M = 64$, and the up-arrows represent the location of a transmitted symbol. The 1024 points correspond to the positive frequencies in the 2048-point discrete spectrum, and T_{smp} is the inverse of the sample rate of the analog-to-digital converter.

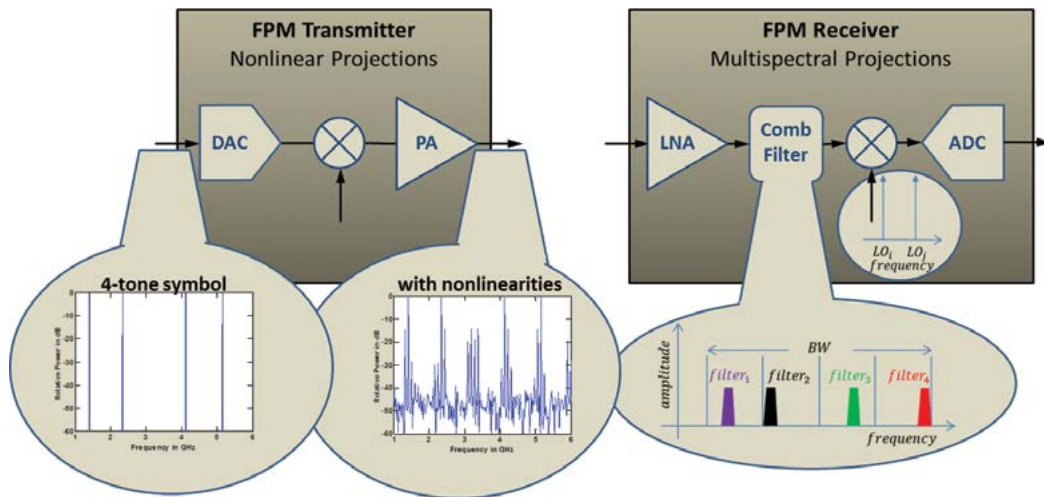


FIGURE 13
 The analog transmit and receive processing chain in FPM. The colored filters represent the comb filter pass-band of the FPM receiver.

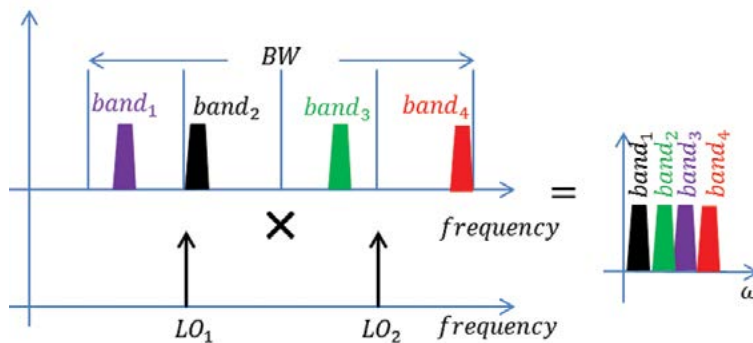


FIGURE 14
 The placement of the LOs with respect to the $N_{pos} = 4$ contiguous bands where FPM symbols have support enable collapsing a wideband spectrum into a narrower one — in the case above at zero-IF prior to digitization — without a loss of information.

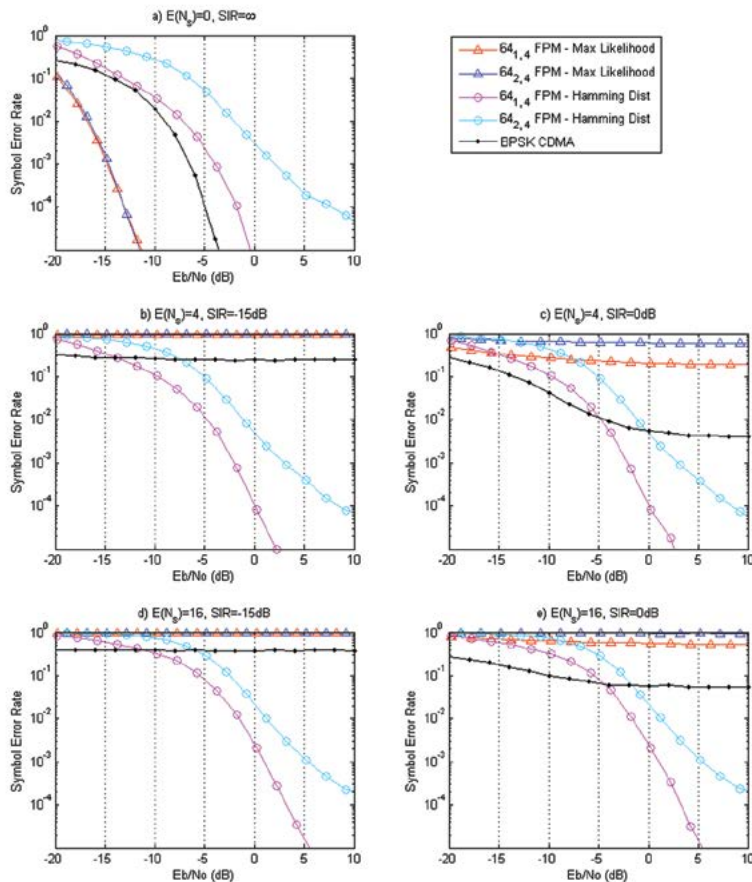


FIGURE 15

The SER performance of FPM vs DS-CDMA. $E(N_i)$ corresponds to the average number of narrowband interference sources present on each Monte Carlo run. SIR is the average signal-to-interference ratio and E_b/N_0 is the ratio of bit energy to noise spectral density.

distance metric significantly outperformed DS-CDMA, which was disproportionately affected by interference due to its wide IBW. Finally, for the same fixed data rate, the processing gain of FPM was roughly an order of magnitude higher than that of DS-CDMA, and this is reflected in the improved SER performance of FPM.

Conclusion: As demonstrated in Fig. 15, FPM is capable of operating in dense interference environments where conventional LPI/LPD communications fail. FPM analog processing used distortions generated by the PA on transmit and wideband undersampling on receive to simultaneously increase both processing gain and data rate. FPM benefits the Navy by providing a robust LPI/LPD communications waveform that can operate in interference-laden environments to ensure high-priority information reaches its intended destination.

[Sponsored by the NRL Base Program (CNR funded)]

References

- ¹ J. Goodman, C. Bertocini, M. Moore, B. Nousain, and G. Cowart, "Frequency Position Modulation Using Multi-Spectral Projections," *Proc. SPIE* **8514**, 85140C (2012).
- ² M. Herman, B. Miller, and J. Goodman, "The Cube Coefficient Subspace Architecture for Nonlinear Digital Predistortion," in *Conference Record of the 42nd Asilomar Conference on Signals, Systems and Computers*, pp. 1857–1861 (IEEE, 2008).
- ³ J. Goodman, K. Forsythe, and B. Miller, "Efficient Reconstruction of Block-Sparse Signals," in *2011 IEEE Statistical Signal Processing Workshop*, pp. 629–632 (IEEE, 2011).

